AECL-12121

ELSEVIER

Journal of Nuclear Materials 294 (2001) 45–52

journal of nuclear materials

www.elsevier.nl/locate/jnucmat

Migration behaviour of iodine in nuclear fuel

W.H. Hocking *, R.A. Verrall, I.J. Muir

Atomic Energy of Canada Limited (AECL), Chalk River Laboratories (CRL), Chalk River, Ont., Canada K0J 1J0

Abstract

A novel out-reactor method has been further developed for investigating the migration behaviour of fission products in UO_2 nuclear fuel, which allows the effects of thermal diffusion, radiation damage and local segregation to be independently assessed. Tailored concentration profiles of any desired species are first created in the near-surface region of polished samples by ion implantation. The impact of either thermal annealing or simulated fission is then precisely determined by depth profiling with high-performance secondary ion mass spectrometry (SIMS). Comparison of iodine migration in UO_2 wafers that had been ion-implanted to fluences spanning five orders of magnitude has revealed subtle radiation-damage effects and a pronounced concentration dependence for thermal diffusion. At concentrations above $\sim 10^{16}$ atoms/cm^3 much of the iodine became trapped, likely in microscopic bubbles. True thermal diffusion coefficients for iodine in polycrystalline UO_2 have been derived by modelling the low-fluence data. © 2001 Published by Elsevier Science B.V.

PACS: 61.72.–y; 61.80.–x; 66.30.–h; 82.80.Ms

1. Introduction

The migration and segregation behaviour of fission products in oxide nuclear fuels are controlling factors for performance and safety throughout the nuclear fuel cycle [1–6]. Release of the fission gases Xe and Kr from the fuel matrix can be sufficient at high burnup to cause overpressure swelling of the fuel element. Several of the volatile fission products, most notably iodine, were implicated in an epidemic of fuel failures caused by stress-corrosion cracking of the Zircaloy sheath during the early operation of power reactors [5]. Transport of fission products from defected fuel elements throughout the heat-transport system of operating reactors can contribute significantly to occupational radiation exposures. Accumulation of segregated fission products on the UO_2 grain boundaries and at the fuel-sheath interface also greatly enhances the potential for release of radioactivity to the environment during postulated accidents and from spent fuel in storage or after disposal [2–4]. Although considerable effort has been expended over the past three decades to develop computer codes for predicting fuel performance under normal and off-normal operating conditions, there is still room for improvement in the physical models and the experimental databases used for this purpose.

Migration to the fuel grain boundaries is the first stage, and normally the rate-limiting step, in any mechanistic model of fission-product segregation and release [3]. Three distinct regimes have been recognized for diffusion of fission products within UO_2 fuels during reactor operation. These are dependent upon whether the two processes necessary for diffusion – formation of vacancies and migration of vacancies – are predominantly controlled by thermal activation or radiation [7]. For temperatures below ~1000 K, diffusion has been shown to be athermal and directly proportional to the fission rate; this radiation-induced diffusion (RID) arises from transient thermal-spike and pressure-gradient effects that occur along fission tracks [8–10]. True thermal diffusion (TD), in which both the formation and migration processes are thermally controlled, predominates only above ~1700 K [7–11]. At intermediate temperatures, vacancies are mainly created by radiation damage, but migration occurs by thermally activated

* Corresponding author. Tel.: +1-613 584 3311; fax: +1-613 584 3250.

E-mail address: hockingw@aecl.ca (W.H. Hocking)

0022-3115/01/$ - see front matter © 2001 Published by Elsevier Science B.V
PII: S0022-3115(01)00447-0

jumps between these lattice sites – providing radiation-enhanced diffusion (RED) [7,11]. The non-equilibrium vacancy concentration is determined by thermal annealing as well as the fission rate. Both TD and RED can be strongly influenced by the stoichiometry of the $UO_{2\pm x}$ matrix (affects vacancy population) and the concentration of impurities (burnup) [11–23]. If the solubility limit of a particular fission product in the uraninite lattice is exceeded, precipitation as microscopic intragranular particles or bubbles can occur. These serve as effective traps or sinks for that fission product, thereby inhibiting migration through the fuel matrix, unless they are disrupted by fission spikes (radiation-induced re-solution) [24,25].

The diffusion of fission products in UO_2 nuclear fuels has been the subject of more than a hundred investigations over the past four decades [7,11–23]. Particular attention has been focussed on the fission gases Xe and Kr, but a number of studies of other volatile fission products have also been reported. Measurements have been performed on irradiated materials with burnups spanning about nine orders of magnitude (10^{11}–10^{20} fissions/cm^3) and extended to even higher equivalent levels by ion implantation [7,11,16,18,23,26]. Although thermal annealing of previously irradiated or ion-implanted samples has been the more commonly used approach [12–23,26], several in-reactor studies have been conducted as well [7,11]. Aside from one microprobe analysis of Cs and Xe gradients within individual grains of irradiated fuel [27], diffusion information has always been derived from measurements of fission-product release, which can be very difficult to interpret properly [15,18,21]. The Booth model has normally been used to analyze the release data obtained from irradiated materials; it yields an effective diffusion coefficient, D/a^2, where a is the radius of a hypothetical sphere equivalent to the diffusion volume [26,28]. For typical polycrystalline ceramic samples, evaluating the appropriate value of this sphere radius introduces considerable additional uncertainty into the final result [15,18,26]. Significant artefacts have also been encountered in studies of the release of ion-implanted radiotracers from polished UO_2 wafers [29]. Direct measurement of the diffusive spreading of a concentrated source, such as a deposited film, has generally been considered the only reliable technique for determination of diffusion coefficients [18,21–23]. This approach has previously been applied only to the lattice constituents (oxygen and actinides) of the oxide nuclear fuels [21,23,30–36].

A novel method that has been developed for investigating the migration behaviour of fission products in UO_2 nuclear fuels is illustrated further here [37]. Progressive changes in the concentration profiles of ion-implanted fission products are precisely determined by depth profiling with high-performance secondary ion mass spectrometry (SIMS). The impact of thermal diffusion, radiation damage and local segregation can be independently assessed. Although the potential of the method has now been demonstrated for several fission products, this paper will focus on iodine. Ion implantation has been extensively used to study diffusion of fission products in oxide nuclear fuels; however, only the release of radiotracers was previously monitored (see references cited in [29]). Despite the fact that it has been well recognized as a powerful technique for characterization of diffusion profiles [38,39], application of SIMS has been limited to the lattice constituents (not ion-implanted) of the oxide nuclear fuels [33,34,36].

2. Experimental procedures

The experiments reported here were mostly performed using polycrystalline UO_2 wafers, ~2 mm thick and ~1.2 cm in diameter, which had been sintered to ~97% of the theoretical density, with polygonal, equiaxed grains, mainly 5–15 μm in size (fuel-grade ceramic). A substantial number of additional samples have also been fabricated from 3 at.% burnup SIMFUEL [40] and UO_2 single crystals; however, only preliminary studies have been conducted so far on either of these materials. Mechanical damage created by polishing one face of each sample to a 0.05 μm finish was removed by thermal annealing at 1500°C in an atmosphere of Ar–4%H_2 [41]. Tailored concentration profiles of stable isotopes of various fission products (including Rb, Kr, Cs, Xe, Eu and Er as well as I) were then introduced into the near-surface region of the polished face by ion implantation.

Thin altered surface films extending to depths of only ~20 nm were obtained by 40 keV ion implantation using an electromagnetic mass separator (at CRL) [29]. Buried layers, with near-Gaussian distributions of fission products, at mean projected ranges of ~75 or ~150 nm, were created by employing ion-implantation energies from 300 keV to 1 MeV. These were initially produced with a Pelletron (at CRL) and later with a tandem accelerator (operated by Interface Science Western at the University of Western Ontario). In all cases, the focussed ion beam was rastered across the sample to ensure uniform implantation and the wafers were divided in two (or sometimes three) to obtain identical duplicate samples. The implanted-ion fluence was varied over five orders of magnitude, from 1.0×10^{11} to 1.0×10^{16} ions/cm^2.

Diffusive spreading of the ion-implanted fission-product layer was caused by either thermal annealing or fission-fragment radiation damage. Thermal annealing was performed in a high-density alumina tube furnace at peak temperatures between 1200°C and 1650°C for periods ranging from 10 min to 24 h. A type B thermocouple was used to monitor the temperature in situ. The oxygen potential within the tube furnace was controlled

by a flowing gas mixture of Ar–4%H_2, which should preserve an almost exactly stoichiometric UO_2 composition [15]. Fission-fragment radiation was simulated by 72 MeV iodine-ion bombardment using a tandem accelerator (at CRL).

The distributions of fission products within both diffused and as-implanted samples were depth-profiled using a Cameca IMS 6f SIMS instrument, which had been customized for safe handling of radioactive materials. A double-focussing magnetic-sector mass spectrometer provides high throughput for secondary ions, which are detected with a channel-electron multiplier operated in the single-ion counting mode. The pressure inside the sample chamber was $<10^{-9}$ Torr during the analyses. A Cs^+ primary-ion beam was used to enhance the yield of negative secondary ions when depth profiling iodine (detected as I^-), whereas sputtering with O_2^- or O^- is normally employed for analysis of electropositive fission products [42]. The focussed 10 keV Cs^+ beam, with a diameter of ~30 μm and a current of 30–100 nA, was rastered over an area of 250 μm by 250 μm on the sample surface. Secondary ions were efficiently collected, using a 5 kV extraction field, from a smaller region (60–100 μm in size) located in the centre of the sputtered area to minimize crater-edge effects [42]. For the low-fluence implants, sensitivity was optimized by selecting a large secondary-ion energy range (~50 eV) spanning the main part of the energy distribution curve [42]. For the high-fluence implants, sensitivity was intentionally degraded somewhat – to avoid saturating the detection system – either by selecting a narrower energy-acceptance window and/or by shifting this window to higher secondary-ion energies, where the yield is much lower.

The depth scale for every sputter profile was subsequently determined by measuring the crater depth using a Tencor Alpha-Step 500 stylus profilometer, which was routinely calibrated against a thin step-height standard (450 ± 3 nm) purchased from VLSI Standards. Significant roughness developed in the bottom of craters sputtered in polycrystalline samples, arising from differences in sputtering rates for the various UO_2 grain orientations [37]. An average crater depth was then derived from a minimum of six line scans recorded across the central region of each crater in two different directions. Because ~100 grains are included in the analysis area, the effects of different grain orientations should be largely averaged out. Depth profiles were always recorded in pairs – one from a diffused sample and one from its as-implanted duplicate – under identical operating conditions. The concentration scale for the as-implanted sample was determined from the integrated area under the profile and the known implantation fluence [42]. A relative sensitivity factor (RSF), for I^- normalized to a matrix species, could then be derived that was appropriate under these conditions [42]. Finally, application of this RSF to the profile for the diffused sample allowed its concentration scale to be calibrated – independent of any loss of iodine due to volatilization from the surface. Generally good agreement was obtained using U^-, UO^- and UO_2^- as the matrix species for the RSF normalization (data reported here are based upon UO^-, but U^- gave almost identical results).

3. Results and discussion

Illustrative SIMS depth profiles of ^{127}I that had been ion-implanted in polycrystalline UO_2 at 900 keV to a fluence of 1×10^{13} ions/cm^2 are displayed in Fig. 1. The changes observed here in the iodine depth distribution after thermal annealing at 1650°C are indicative of three separate diffusion phenomena. Migration of the iodine toward greater depths in the tail of the profile, which increases as a function of the annealing time, is consistent with thermal diffusion. For iodine concentrations above ~10^{16} atoms/cm^3, there is no evidence of diffusive

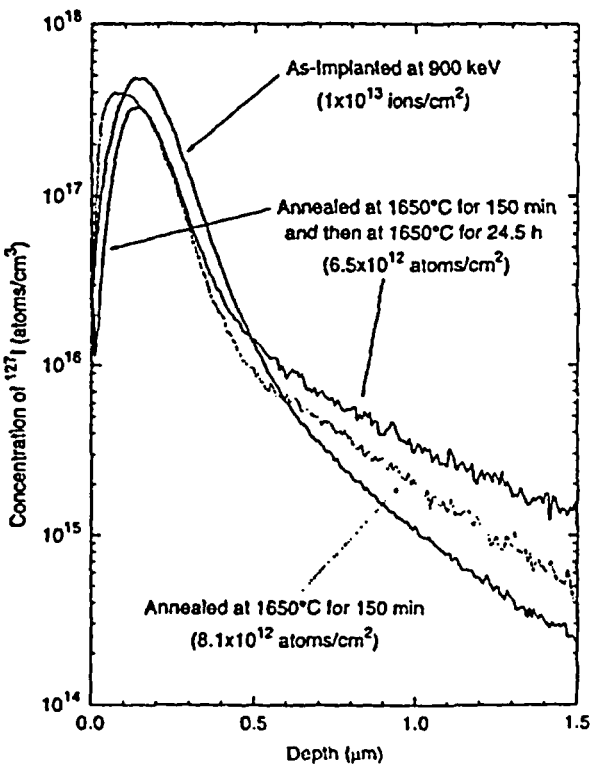

Fig. 1. Suite of SIMS depth profiles of ^{127}I that had been ion-implanted in polycrystalline UO_2 at 900 keV to a fluence of 1×10^{13} ions/cm^2; the as-implanted distribution as well as the changes caused by thermal annealing at 1650°C for 150 min and then 24.5 h are shown. The numbers in parentheses are the retained fluences.

spreading into the bulk matrix, which indicates trapping at relatively immobile defect sites. Finally, shifting of the peak in the iodine distribution toward the surface after the first anneal has been interpreted in terms of a specialized form of RED associated with lattice vacancies created during the implantation process [37].

A threshold of $\sim 10^{16}$ atoms/cm^3 for iodine trapping in UO_2 has been confirmed through several additional experiments performed on single-crystal as well as polycrystalline samples using a range of annealing periods (10 min–24 h) and temperatures (1200–1650°C). At a concentration of 10^{16} atoms/cm^3, the mean distance between as-implanted iodine atoms is ~45 nm, which is more than the estimated mean diffusion distance at the lower temperatures and shorter times. A threshold of $\sim 10^{16}$ fissions/cm^3, which represents a burnup of only ~0.01 MW h/kg U, has also been found for trapping of xenon during post-irradiation thermal annealing of single-crystal and polycrystalline UO_2 samples [16,18,23]. This corresponds to a xenon concentration of only $\sim 3 \times 10^{15}$ atoms/cm^3, because xenon represents ~15% of the total fission-product inventory and each fission creates two fragments, but the combined concentrations of all fission products with negligible solubility in the uraninite lattice would still exceed 10^{16} atoms/cm^3. Trapping of insoluble diffusing species is controlled by the abundance of defects in the matrix as well as the concentration of impurities [16]. The lowest energy site for both iodine and xenon atoms in the UO_2 lattice is a uranium vacancy combined with one or two oxygen vacancies, and a second uranium vacancy is thought to be involved in the migration process [43–48]; however, a cluster of more than two uranium vacancies (along with associated oxygen vacancies) would provide an effective trap for insoluble fission products. Unless they are occupied by impurity atoms and/or coalesce into microscopic pores, small vacancy clusters will mostly be annihilated at temperatures where thermal diffusion is appreciable through recombination with uranium and oxygen interstitials [49]. The energy of fission products (67–95 MeV) is predominantly transferred to the fuel matrix via electronic excitations (~95%), whereas ion implantation at ~1 MeV involves substantial nuclear stopping (~50%). Calculated estimates of the initial number of uranium vacancies created by these two processes differ by only about one order of magnitude (~27 000 per fission versus ~2100 per 900 keV implanted I ion) [8,50,51]. Furthermore, thermal-spike and pressure-gradient effects along fission tracks have been shown to anneal out ~80% of the initial defects [8,50]. Although thermal-spike effects have been inferred for less energetic ions as well [29], lattice-damage measurements indicate that the recombination efficiency is considerably lower within the nuclear-stopping regime [8,52]. These considerations provide a plausible rationale for why the two quite different processes for introducing insoluble impurities into the UO_2 matrix – fission and ion implantation at <1 MeV – should provide comparable trapping thresholds.

Penetration of 900 keV ^{127}I ions into a UO_2 matrix has been modelled using the SRIM-2000 simulation code, which is based upon a quantum mechanical treatment of ion-atom collisions [51]; calculated depth distributions of implanted iodine atoms and lattice vacancies have been reproduced in Fig. 2. The mean projected range of the iodine here (150 nm) agrees well with the peak in the depth distributions measured by SIMS for the as-implanted standard (143 nm with a 3 nm standard deviation of the mean). Damage caused by recoil collisions is greatest at shallower depths than the iodine mean projected range: the calculated populations of uranium and oxygen vacancies both reach their maximum within 100 nm of the surface. Preferential migration of iodine from greater depths into this high-damage zone would cause not only the measured shift in the peak position but also the observed asymmetry in the profile (see curve for 150 min anneal in Fig. 1). Additional experiments conducted using lower temperatures and shorter annealing times (on polycrystalline UO_2 samples ion-implanted with ^{127}I to a fluence of 1×10^{13} ions/cm^2) revealed that the directed migration

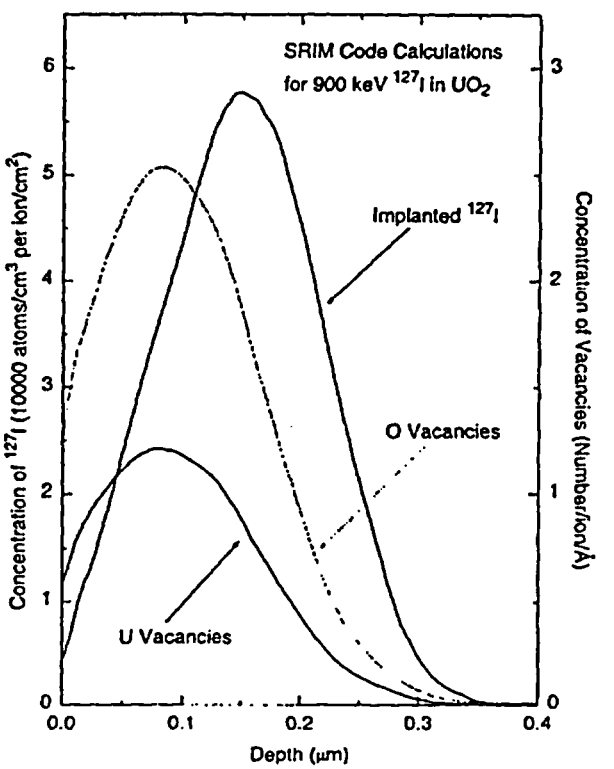

Fig. 2. Depth distributions of implanted iodine atoms and lattice vacancies in a UO_2 matrix calculated using the SRIM-2000 simulation code for 900 keV ^{127}I ion bombardment.

started near 1200°C and was fully developed after 10 min at 1465°C [37]. This is consistent with the expectation that the radiation damage to the uranium lattice should be largely removed by annealing at these lower temperatures [49]. Evidently, the redistribution toward the surface seen in Fig. 1 must have occurred rapidly during the initial stages of the first anneal before most of the iodine became trapped. Prolonged annealing at 1650°C (curve for 24.5 h in Fig. 1) caused a modest further reduction in the integrated iodine concentration and significant restoration of the profile symmetry, which can be reasonably attributed to release of iodine from the surface (but see also below).

Depth profiles of ^{127}I that had been ion-implanted in polycrystalline UO_2 to a fluence of 1×10^{16} ions/cm^2 are shown in Fig. 3. No evidence of thermal diffusion of iodine into the bulk is seen here, even after the 1650°C anneal – consistent with the trapping threshold of $\sim 10^{16}$ atoms/cm^3 found above. These data were collected using conditions optimized for the peak iodine concentration, but it is unlikely that sufficient dynamic range could have been achieved with maximum sensitivity to follow the iodine below 10^{16} atoms/cm^3 in the tail of the distribution [42]. A small shift in the peak of the iodine distribution toward the surface is already apparent in Fig. 3 after the short initial anneal at 1200°C. This again becomes more pronounced following the 1650°C anneal, but is now accompanied by a more significant decrease in the integrated iodine concentration (compare Figs. 1 and 3). Enhanced release of iodine from the surface because of the greater damage caused by the higher fluence is likely; however, coalescence of iodine traps into microscopic bubbles also now seems probable. Formation of bubbles several nanometres in size has been previously demonstrated (using transmission electron microscopy) within UO_2 single crystals that had been ion-implanted with ^{127}I at 40 keV to a fluence of 10^{16} ions/cm^2 and then annealed at temperatures up to 1500°C [53]. During the SIMS depth profiling, the yield of I^- ions from such bubbles would almost certainly be different from, and most likely lower than, the yield of I^- ions from individual iodine atoms or clusters trapped in the UO_2 matrix.

Clear thermal diffusion of iodine into the bulk UO_2 matrix is illustrated in Fig. 4, which displays depth

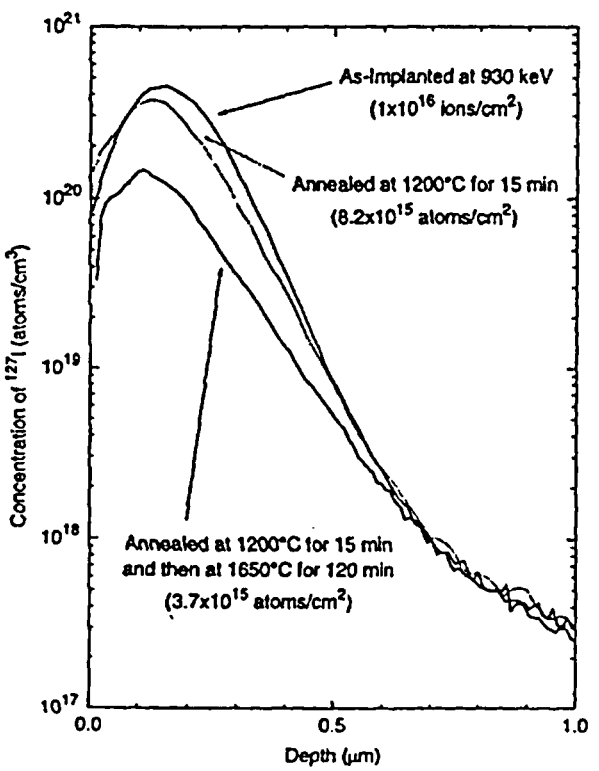

Fig. 3. Suite of SIMS depth profiles of ^{127}I that had been ion-implanted in polycrystalline UO_2 at 930 keV to a fluence of 1×10^{16} ions/cm^2; the as-implanted distribution as well as the changes caused by thermal annealing at 1200°C for 10 min and then at 1650°C for 120 min are shown.

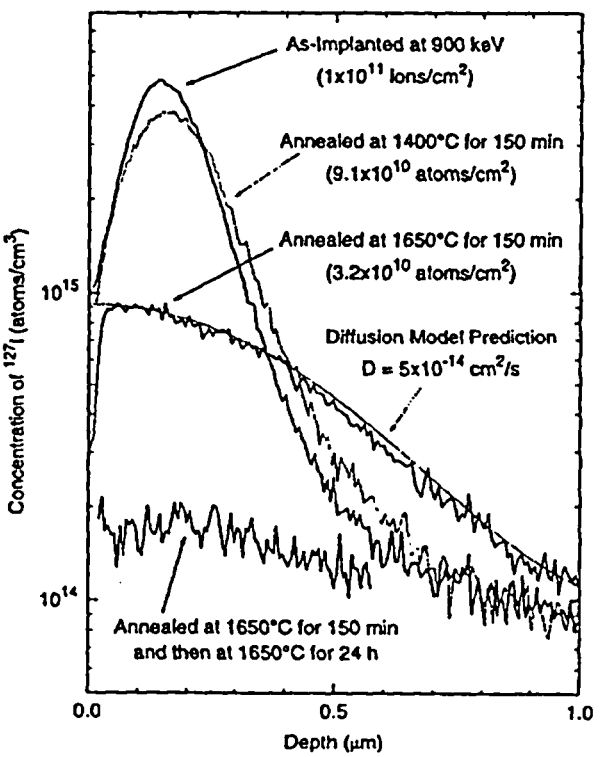

Fig. 4. Depth profiles of ^{127}I as-implanted in polycrystalline UO_2 at 900 keV to a fluence of 1×10^{11} ions/cm^2 and after thermal annealing either at 1400°C for 150 min or at 1650°C for 150 min and then 24 h. The profile following the second anneal at 1650°C has not been shown beyond a depth of ~0.6 μm for clarity (it converges on the as-implanted profile). A diffusion model prediction for the 150 min anneal at 1650°C has also been displayed.

profiles of ^{127}I as-implanted at 900 keV to a fluence of 1×10^{11} ions/cm^2 and after thermal annealing either at 1400°C for 150 min or at 1650°C for 150 min and then 24 h. The peak iodine concentration here ($<5 \times 10^{15}$ atoms/cm^3) is below the trapping threshold identified above ($\sim 10^{16}$ atoms/cm^3). Duplicate profiles collected from the annealed samples demonstrated excellent reproducibility. Although the effective iodine diffusion distance for the lower temperature anneal is still only a fraction of the mean implanted depth, there is no doubt that the entire profile shape has been affected. The higher temperature and longer annealing period caused a progressive increase in the extent of the iodine redistribution.

Diffusive spreading of the low-fluence iodine implants was modelled initially using the Mathcad software package (Mathsoft, Cambridge, MA, USA); an analytical solution for diffusion of an arbitrary distribution of solute into a semi-infinite medium, with solute evaporation from the surface in proportion to the concentration there, was adapted from the heat-flow formula of Carslaw and Jaeger [54]. The same result was subsequently achieved by numerically solving Fick's law (differential equation) using the Mathematica software package (Wolfram Research, Champaign, IL). As illustrated in Fig. 4 for the 150 min anneal at 1650°C, reasonably good fits to the altered iodine distributions could be achieved. Thermal diffusion coefficients of 3×10^{-15} and 5×10^{-14} cm^2/s were thus obtained for 1400°C and 1650°C respectively; however, these numbers are regarded as preliminary until confirmed by further experiments and a more thorough overall assessment. The smaller coefficient falls at the low end of the range of previously reported values derived from in-reactor iodine release measurements at 1400°C, which span two orders of magnitude [7,11,55], but nearly coincides with selected results (4×10^{-15} and 5×10^{-15} cm^2/s) for small UO_2 single crystals [7]. This agreement may be partly fortuitous as the in-reactor migration data reflect the competing influences of trapping and radiation-enhancement on thermal diffusion. Post-irradiation measurements of iodine release from polycrystalline samples have been performed at higher temperatures, but even the derived D/a^2 values span three orders of magnitude and there is the additional uncertainty of choosing an appropriate radius for the Booth spheres [15,26,56]. A recent theoretical analysis of iodine migration in UO_2 concluded that the controlling process would likely be uranium self-diffusion and inferred rather smaller diffusion coefficients [48].

The impact of bombardment with 72 MeV iodine ions on the depth distribution of ^{127}I that had been previously ion-implanted at 930 keV to a fluence of 1×10^{13} ions/cm^2 is shown in Fig. 5. A linear-log background has been subtracted from the altered profiles to correct for a slight excess of iodine in this

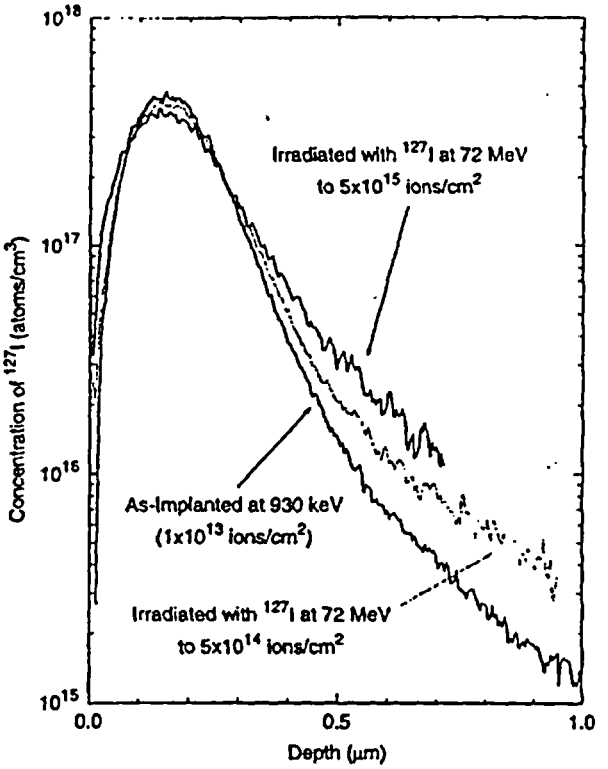

Fig. 5. Depth profiles of ^{127}I as-implanted in polycrystalline UO_2 at 930 keV to a fluence of 1×10^{13} ions/cm^2 and after irradiation with ^{127}I at 72 MeV to fluences of 5×10^{14} and 5×10^{15} ions/cm^2. A linear-log background has been subtracted from the altered profiles.

region arising from the high-energy ion bombardment. Although the vast majority of the 72 MeV iodine ions come to rest within ±1 μm of the mean projected range (6.3 μm), there is a long tail on the distribution that extends right back to the surface owing to occasional direct-impact collisions with the nuclei of lattice atoms. The observed spreading of the implanted-ion profile, which increases as a function of the 72 MeV ion fluence, provides an explicit demonstration of RID. Migration of iodine here at concentrations well above the defect-trapping threshold identified for thermal diffusion is a further indication of the importance of radiation-damage effects for fission-product segregation. Approximate fits of the profiles in Fig. 5 over the 0.05–0.4 μm depth range yielded D^*t values of $\sim 7 \times 10^{-12}$ and $\sim 2 \times 10^{-11}$ cm^2 for the low-fluence and high-fluence irradiation respectively, where D^* is an effective diffusion coefficient for RID and t is time. At greater depths the altered distribution profiles are rather uncertain because of the background subtraction and there may also be some contribution from recoil implantation caused by direct-impact collisions.

The RID coefficient for in-reactor fission has been shown to be independent of temperature and directly proportional to the fission rate, $D^* = A(f/t)$, where f is the number of fissions per unit volume and A is a constant with units of length to the fifth power [7–10]. Accelerator fluence (F) can then be related to fission using the expression $F = 2f\delta$, where δ is the mean length of a fission track and the factor of 2 arises from allowing for two fragments per fission that produce thermal spikes of finite volume when integrating over all possible fission-fragment directions. An A value of $0.5–2 \times 10^{-29}$ cm^5 was then derived from the D^*t measurements above with $\delta = 6.3$ μm (the mean projected range of 72 MeV ^{127}I ions in UO_2 calculated using the SRIM code) [51]. This agrees well with the results from studies of RID of metal lattice atoms in UO_2 and $(U,Pu)O_2$ by α-spectrometry depth profiling of thin tracer layers (1.5×10^{-29} and 1.2×10^{-29} cm^5 respectively) [9,57]. In-reactor measurements of iodine release have indicated a somewhat smaller A value ($0.5–3 \times 10^{-30}$ cm^5) and similar findings have been reported for krypton and xenon [7,11]; however, because these samples had been previously annealed at 1400°C over extended irradiation periods, the athermal release must reflect bubble re-solution as well as single-atom diffusion.

4. Conclusions

A novel method has been further developed for investigating the migration behaviour of fission products in UO_2 nuclear fuels, which allows the effects of thermal diffusion, radiation damage and local segregation to be independently assessed. Direct evidence has been obtained for RED associated with lattice vacancies created by collision cascades during the initial implantation. A threshold of $\sim 10^{16}$ atoms/cm^3 has been determined for iodine trapping at defect sites in the UO_2 matrix, which is consistent with out-reactor measurements of fission-gas release from trace-irradiated fuels. RID of iodine in UO_2 has been simulated by bombardment with 72 MeV iodine ions. These findings provide additional confirmation that radiation-damage effects must play a crucial role in the redistribution of fission products within oxide nuclear fuels. Preliminary TD and RID coefficients derived for iodine, at 1400°C and low temperatures respectively, agree with selected in-reactor data to within a factor of two.

Acknowledgements

The authors would like to acknowledge the participation of S.J. Bushby and P.G. Lucuta in the early stages of these studies. They would also like to thank H.R. Andrews, L.E. Bahen, J.D. Bonnett, J.F. Mouris, H.H. Plattner and T. Simpson for their contributions to various aspects of the sample preparation, ion-implantation and simulated fission-product damage. The authors are grateful to R.S. Dickson for reviewing the manuscript and to Hj. Matzke for extensive consultation and advice on diffusion of fission products in nuclear fuels.

References

[1] H. Kleykamp, J. Nucl. Mater. 131 (1985) 221.
[2] J.R. Matthews, J. Chem. Soc. Faraday Trans. 2 83 (1987) 1273.
[3] J.H. Gittus, J.R. Matthews, P.E. Potter, J. Nucl. Mater. 166 (1989) 132.
[4] L.H. Johnson, D.W. Shoesmith, in: W. Lutze, R.C. Ewing (Eds.), Radioactive Waste Forms for the Future, Elsevier, Amsterdam, 1988, p. 635 (Ch. 11).
[5] B. Cox, J. Nucl. Mater. 172 (1990) 249.
[6] W.H. Hocking, A.M. Duclos, L.H. Johnson, J. Nucl. Mater. 209 (1994) 1.
[7] J.A. Turnbull, C.A. Friskney, J.R. Findlay, F.A. Johnson, A.J. Walter, J. Nucl. Mater. 107 (1982) 168.
[8] Hj. Matzke, Radiat. Eff. 64 (1982) 3.
[9] Hj. Matzke, Radiat. Eff. 75 (1983) 317.
[10] T. Wiss, Hj. Matzke, C. Trautmann, M. Toulemonde, S. Klaumunzer, Nucl. Instrum. and Meth. B 122 (1997) 583.
[11] M. Hirai, J.H. Davies, R. Williamson, J. Nucl. Mater. 226 (1995) 238.
[12] R. Lindner, Hj. Matzke, Z. Naturforsch. 14a (1959) 582.
[13] W. Miekeley, F.W. Felix, J. Nucl. Mater. 42 (1972) 297.
[14] J.C. Killeen, J.A. Turnbull, in: K.A. Simpson, P. Wood (Eds.), Proceedings of the Workshop on Chemical Reactivity of Oxide Fuel and Fission Product Release, Berkeley, UK, vol. 2, CEGB, 1987, p. 387.
[15] M.A. Mansouri, D.R. Olander, J. Nucl. Mater. 254 (1998) 22.
[16] J.R. MacEwan, W.H. Stevens, J. Nucl. Mater. 11 (1964) 77.
[17] G.T. Lawrence, J. Nucl. Mater. 71 (1978) 195.
[18] Hj. Matzke, Radiat. Eff. 53 (1980) 219.
[19] K. Une, I. Tanabe, M. Oguma, J. Nucl. Mater. 150 (1987) 93.
[20] K. Une, S. Kashibe, J. Nucl. Sci. Technol. 27 (1990) 1002.
[21] Hj. Matzke, J. Chem. Soc. Faraday Trans. 2 83 (1987) 1121.
[22] Hj. Matzke, Advances in Ceramics, Vol. 17, Fission-Product Behaviour in Oxide Nuclear Fuel, American Ceramics Society, Westerville, OH, 1986, p. 1.
[23] Hj. Matzke, in: R.P. Agarwala (Ed.), Diffusion Processes in Nuclear Materials, Elsevier, Amsterdam, 1992, p. 9.
[24] J.A. Turnbull, R.M. Cornell, J. Nucl. Mater. 41 (1971) 156.
[25] H. Blank, Hj. Matzke, Radiat. Eff. 17 (1973) 57.
[26] S.G. Prussin, D.R. Olander, W.K. Lau, L. Hansson, J. Nucl. Mater. 154 (1988) 25.
[27] C.T. Walker, K. Lassman, J. Nucl. Mater. 138 (1986) 155.
[28] A.H. Booth, Atomic Energy of Canada Limited Reports, AECL-496/CRDC-721 and AECL-700/DCI-27, 1957.

[29] W.H. Hocking, R.A. Verrall, P.G. Lucuta, Hj Matzke, Radiat. Eff. Defects Solids 125 (1993) 299.
[30] R.J. Hawkins, C.B. Alcock, J. Nucl. Mater. 26 (1968) 112.
[31] J.F. Marin, P. Contamin, J. Nucl. Mater. 30 (1969) 16.
[32] Hj. Matzke, J. Nucl. Mater. 30 (1969) 26.
[33] K.C. Kim, D.R. Olander, J. Nucl. Mater. 102 (1981) 192.
[34] G.E. Murch, C.R.A. Catlow, J. Chem. Soc. Faraday Trans. 2 83 (1987) 1157.
[35] P.J. Hayward, I.M. George, R.A. Kaatz, D.R. Olander, J. Nucl. Mater. 244 (1997) 36.
[36] A.C.S. Sabioni, W.B. Ferraz, F. Millot, J. Nucl. Mater. 257 (1998) 180.
[37] W.H. Hocking, R.A. Verrall, S.J. Bushby, International Atomic Energy Agency Report, IAEA-TECDOC-1122, 1999, p. 111.
[38] M.P. Macht, V. Naundorf, J. Appl. Phys. 53 (1982) 7551.
[39] J.A. Kilner, Mater. Sci. Forum 7 (1986) 205.
[40] P.G. Lucuta, R.A. Verrall, Hj. Matzke, B.J. Palmer, J. Nucl. Mater. 178 (1991) 48.
[41] Hj. Matzke, A. Turos, J. Nucl. Mater. 114 (1983) 349.
[42] R.G. Wilson, F.A. Stevie, C.W. Magee, Secondary Ion Mass Spectrometry: A Practical Handbook for Depth Profiling, Wiley, New York, 1989.
[43] Hj. Matzke, J.A. Davies, J. Appl. Phys. 38 (1967) 805.
[44] C.R.A. Catlow, Proc. R. Soc. London A 364 (1978) 473.
[45] R.G.J. Ball, R.W. Grimes, J. Chem. Soc. Faraday Trans. 86 (1990) 1257.
[46] R.W. Grimes, R.G.J. Ball, C.R.A. Catlow, J. Phys. Chem. Solids 53 (1992) 475.
[47] S. Nicoll, Hj. Matzke, C.R.A. Catlow, J. Nucl. Mater. 226 (1995) 51.
[48] G. Busker, R.W. Grimes, M.R. Bradford, J. Nucl. Mater. 279 (2000) 46.
[49] Hj. Matzke, O. Meyer, A. Turos, Radiat. Eff. Defects Solids 119–121 (1991) 885.
[50] J. Soullard, A. Alamo, Radiat. Eff. 38 (1978) 133.
[51] J.F. Ziegler, J.P. Biersack, U. Littmark, The Stopping and Range of Ions in Solids, Pergamon, New York, 1985 and SRIM-2000 Code at www.research.ibm.com/ionbeams.
[52] W.J. Weber, J. Nucl. Mater. 98 (1981) 206.
[53] V.F. Chkuaseli, Hj. Matzke, J. Nucl. Mater. 223 (1995) 61.
[54] H.S. Carlslaw, J.C. Jaeger, Conduction of Heat in Solids, 2nd Ed., Clarendon, Oxford, 1959, p. 359.
[55] C.A. Friskney, J.A. Turnbull, J. Nucl. Mater. 79 (1979) 184.
[56] D. Davies, G. Long, W.P. Stanaway, United Kingdom Atomic Energy Authority Report, AERE-R-4342, 1963.
[57] A. Hoh, Hj. Matzke, J. Nucl. Mater. 48 (1973) 157.